JET–R(99)06

L C Ingesson

Comparison of Methods to Determine the Total Radiated Power in JET

JET–R(99)06

Comparison of Methods to Determine the Total Radiated Power in JET

L C Ingesson.

JET Joint Undertaking, Abingdon, Oxfordshire, OX14 3EA,

ABSTRACT

Methods to determine the total electromagnetic power, radiated by the plasma, from bolometer measurements are compared. The effectiveness of weighted summations of a limited number of measurements is compared with the values calculated from tomographic reconstructions. The sensitivity of the tomographic reconstructions to various reconstruction parameters and different numbers of lines of sight has also been investigated. The results show that of plasmas with an X point it seems not to be possible to find weights for the weighted summation that give satisfactory results for wide range of plasma parameters. The total radiated power determined from tomographic reconstructions, in contrast, is fairly insensitive to reconstruction parameters, except if negative values are allowed in the reconstructions or if there are inconsistencies between measurements. Beam widths are shown to play only a minor role in the total power calculation.

1. INTRODUCTION

The total radiated power is an important plasma parameter that is required routinely during operations and in the analysis of discharges. The total radiated power can be estimated in various ways, ranging from a simple weighted summation of bolometer lines of sight that can be calculated between discharges, to an elaborate tomographic reconstruction that requires input by hand and can only be carried out for a limited number of time slices in a limited number of discharges. In the past, in JET the simple weighted summation has proven adequate for most purposes and differences between calculation methods could be explained and gave no cause for concern. However, no systematic study comparing the different calculation methods had been carried out. Recent doubts raised by the ASDEX-Upgrade team [1] warrant such a systematic comparison.

The present document describes some relevant technical details of the bolometer diagnostics (Sec.2) and discusses the results obtained with various calculation methods to estimate the total radiated power: by tomographic reconstructions (Sec.3) and by weighted summation of line integrals (Sec.4). The comparison of the methods is mainly done by means of simulations with realistic phantoms, i.e. emission profiles that are expected to occur in JET. The phantoms used in this study are the emission profiles predicted by the EDGE2D/NIMBUS code for the attached and detached phase of an L-mode density-limit discharge in the MkIIA divertor. The methods have also been compared with experimental data for a variety of discharges in different divertors. In addition, the effects on the calculated total radiated power due to the finite width of the instrument functions (beam width) are studied in Sec.5.

2. TECHNICAL DESCRIPTION OF THE BOLOMETER DIAGNOSTICS

2.1 Bolometers of the KB1, KB3 and KB4 systems

Three bolometer systems are in use on JET: three 10 or 14-channel ex-vessel KB1 cameras (Fig.1), 14 4-channel in-vessel KB4 cameras (Fig.2), and 7 4-channel in-vessel KB3 cameras in

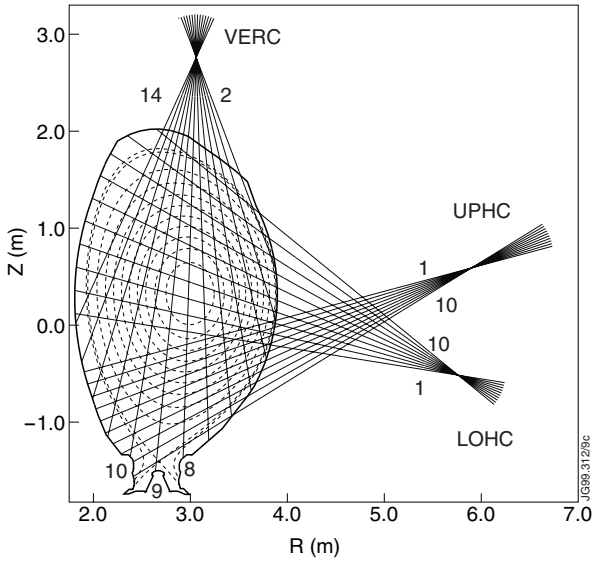

Fig.1: Lines of sight of the three cameras of the KB1 bolometer system. The dotted curves indicate typical flux surfaces.

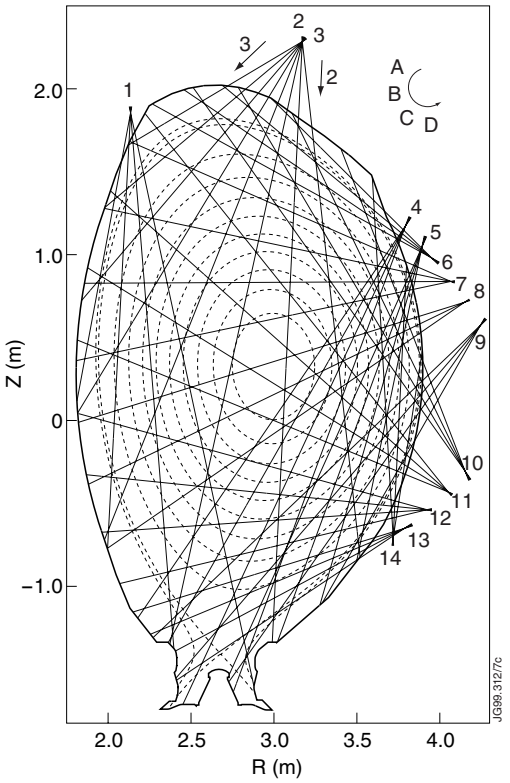

Fig.2: Lines of sight of the 14 cameras of the KB4 bolometer system.

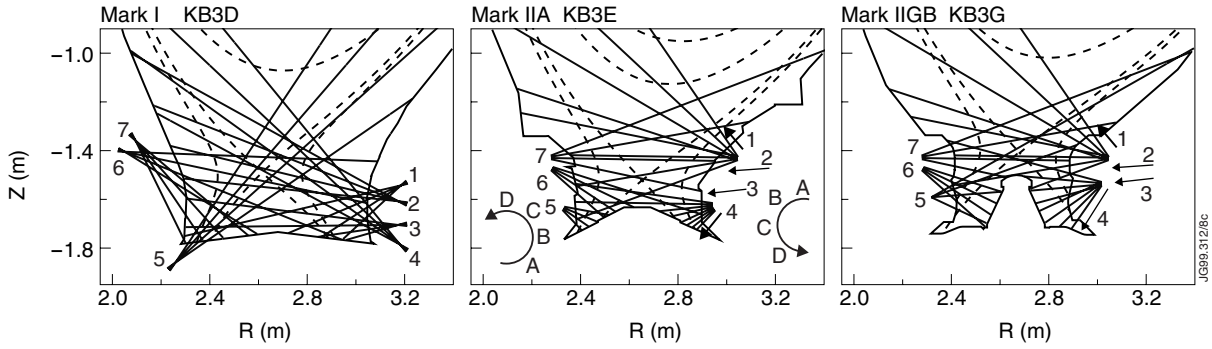

Fig.3: Lines of sight of the seven cameras of the KB3 bolometer system in three divertors.

the divertor (Fig.3). The KB1 system, which is mounted in ports of the vacuum vessel, has been in operation since 1984 and uses single-bolometer assemblies developed at IPP-Garching [2,3]. The radiation is absorbed by an unblackened gold absorber on a Kapton substrate. The resistance change of a resistor mounted on the rear of the Kapton substrate is measured in a measuring bridge, in which also the resistor of a reference bolometer, which is mounted directly behind the signal bolometer, is included. The reference bolometer makes it possible to subtract heating effects by, for example, fusion neutrons and gamma radiation, which are registered by both the signal and reference bolometer. The bolometers are cooled to about room temperature.

The KB3 and KB4 systems use 4-channel bolometer arrays that are mounted in-vessel. The bolometers are based on a newer type of bolometers than the ones of KB1, also developed

at IPP Garching [4]. For application on JET, the bolometers were further developed with a mica substrate instead of Kapton in order that the bolometers do not need to be cooled. Most channels of the KB3 and KB4 systems have operated reliably for several years at 320ºC. These bolometers have a blackened gold absorber. Behind the mica substrate there are two (signal) resistors, and there are also two (reference) resistors behind an identical gold absorber, shielded from radiation, located close to the signal bolometer. The signal and reference resistors are connected in a Wheatstone bridge. All absorbers and resistors of the four channels of the array are on the same mica foil, and, because they have undergone the same processing steps in their manufacture, they are nearly identical.

2.2 Calibration

Both types of bolometer can be calibrated *in situ*, without the need of a calibrated radiation source, by heating up the resistors with a known current and measuring the time response of the output signal [2,4]. Comparison with a calibration with light sources have shown that the above calibration method is satisfactory, although a small correction is needed for the KB1 system [2]. The gold absorber absorbs all radiation in the UV to soft x-ray range. A blackening of the foil extends the good absorption to the visible range. Because of this wide range of sensitivity, most of the radiation emitted by the plasma will be detected. The plasma is optically thin for electromagnetic radiation in this range. Therefore, a good estimate of the total radiated power can be obtained, on the condition that the radiation is toroidally symmetric (the vertical and horizontal KB1 cameras, and the KB3 and KB4 systems are located in different octants). The bolometer systems also detect neutral particles produced in the plasma by charge-exchange processes. Although these play a role in the bulk plasma, the main contribution to the bolometer signals and to the power loss from the plasma comes from the divertor [5–7]. The bulk plasma is opaque to neutral particles, and the coverage by the divertor bolometers is insufficient to fully quantify the total power carried by the neutral particles in the divertor. Therefore, the estimates of total radiated power discussed here only include the electromagnetic radiation part (and a small component of neutral particle losses from the bulk plasma). In tomographic reconstructions, the contribution of neutral particles to the signals of the divertor bolometers (KB3) has to be taken into account [6,7], which complicates the tomographic reconstructions significantly and also makes the results of the total radiated power somewhat less reliable if KB3 measurements are taken into account (but the details of the radiation pattern in the divertor are hugely improved by taking into account the KB3 measurements).

2.3 Coverage and geometric effects

The KB1 and KB4 cameras are pin-hole cameras, i.e. the detectors of one camera view the plasma through one aperture. Due to the limited space in the divertor, the KB3 cameras (in MkIIA and MkIIGB) are collimator cameras, i.e. each detector views the plasma through a number of apertures that are not shared with other detectors. The size of the apertures and location

of the detectors determines the separation between the lines of sight of that camera and the beam widths around the lines of sight from which radiation is received by the detectors. The beam-widths, which are related to the étendue of the detector [8], determine the amount of light that is received, and therefore the signal-to-noise ratio. These quantities and the coverage have been optimized such that there are no gaps not covered between the lines of sight (see Sec. 5). The beam widths are so large that a significant blurring occurs if the emission profile is very localized and peaked. For a proper quantification of the local emissivity it is important to take these beam widths into account (see Ref. 8 and Sec. 3 of this document), although the poor coverage of the plasma severely limits the resolution that can be obtained. In Sec. 5 it is shown that the beam widths have a negligible effect on the total radiated power calculation.

2.4 Reliability of channels

Over the years of operation, several channels of the bolometer systems have ceased to function. Table I gives an overview of the number of channels that are currently working. The main problem in the KB3 and KB4 systems is the crimped connection that is used between the cables leading to the bolometer head and the gold wires that lead to the bolometer foil. Repeated cooling-down and heating-up of the bolometers causes more and more of these crimped connections to fail. Three new divertor bolometers, installed in 1998 for the MkIIGB divertor campaign, have a more reliable design.

Table I: Typical number of working channels of the JET bolometer systems in 1998/1999

System	Total channels	Reliable	Unreliable	Broken
KB1V	14	11	2	1
KB1U, KB1L	20	18	2	-
KB3	28	15	5	8
KB4	56	28	10	18

2.5 Summary

Although the KB1 and KB3/4 systems have different types of bolometers, different electronics, the *in-situ* calibration is achieved in different ways, KB1 has unblackened and KB3/4 blackened absorbers, and the systems are located in different octants, the measurements of these systems are in reasonable agreement. Unfortunately, there are only a very small number of nearly coinciding lines of sight (with different beam widths) that can be compared directly. Overall comparisons, however, do not give any indication that either of the systems measures systematically different values.

In ASDEX-Upgrade significantly higher radiated fractions are obtained than in JET [6,9]. It is important to make sure that systematic errors in the measurements and in the processing are not responsible for this discrepancy, and that the cause must be sought in the plasma behaviour.

Instrumental effects can be ruled out for JET: two different systems give consistent measurements. Furthermore, in some JET plasmas a radiated fraction of up to 100% can be achieved (mainly in some limiter plasmas, but also in some divertor plasmas), which makes systematic errors unlikely. Also, no radiation can escape detection due to the overlap of the viewing beams of adjacent channels. The bolometers used in JET and ASDEX-Upgrade are very similar (although the ASDEX-Upgrade bolometers are unblackened), which makes it likely that the quantities that are compared are indeed comparable (the systems have the same sensitivity range, for example). In JET large neutral charge-exchange particle losses are reported [5–7], levels that are confirmed by EDGE2D/NIMBUS simulations, which may explain the reduced electromagnetic radiated power fraction in JET when the neutral losses are high. The aim of this document is to investigate whether systematic errors are made with the methods used at JET to calculate the total radiated power from the bolometer measurements.

3. TOMOGRAPHY

3.1 Background

If $g(R,Z)$ is the emission profile, where R is the major radius and Z the height above the midplane, i.e. Cartesian coordinates of a poloidal cross-section, line-integral measurements are given by

$$f(p,\xi) = \iint g(R,Z)\,\delta(p + (R - R_0)\sin\xi - (Z - Z_0)\cos\xi)\,\mathrm{d}R\,\mathrm{d}Z\,, \qquad (1)$$

where (R_0, Z_0) is a chosen origin, for example the magnetic axis, and (p,ξ) parametrize a line of sight and are coordinates of projection space: p is the signed distance from the origin to the line and ξ is the angle of the line with the positive R axis. The image $f(p,\xi)$ for a given emission profile $g(R,Z)$, i.e. values $f(p,\xi)$ for (p,ξ) on a regular grid, is called the sinogram of $g(R,Z)$. The range of (p,ξ) is usually chosen as follows: $-a \le p \le a$, where a is the maximum distance from the origin (R_0, Z_0) for which $g(R,Z)$ is nonzero, and $0 \le \xi < \pi$. Sometimes, when the viewing direction is relevant, one can consider $0 \le \xi < 2\pi$; in that case one has to realise that the function $f(p,\xi)$ is subject to "Möbius" periodicity: $f(p,\xi+\pi) = f(-p,\xi)$.

In reality the measurements are not along infinitely thin lines and an instrument function has to be taken into account. If all detectors have identical instrument functions (shift-invariant), $\hat{f}(p,\xi)$, i.e. $f(p,\xi)$ blurred by the instrument function, can be considered. The lines of sight of the JET bolometer system, however, cover the poloidal plane very irregularly (Figs.1–3) and all channels have different instrument functions. Therefore the measurements $\hat{f}_i$ in discrete points corresponding to the average line of sight $(\overline{p}_i, \overline{\xi}_i)$, have to be considered.

The sparse and irregular coverage of the plasma and the very localized and peaked emission in the divertor make tomographic reconstructions of the bolometer measurements difficult. The most successful tomographic inversion algorithm used for bolometry at JET is a constrained-

optimization method that uses smoothness as object function[1] and the discrepancy principle as constraint [6,10]. The method is based on the algorithm used at ASDEX-U [11], but it has several important additions: (1) the discrepancy principle is used to find the regularization parameter (or equivalently, the Lagrange multiplier) [6,10], which means that the values that would be measured if the emission profile obtained by the tomographic reconstruction were true correspond to the actual measurements within estimated error bars; (2) a non-negativity constraint is used to avoid negative emissivities in the reconstruction [10,12][2]; (3) the beam widths are fully taken into account instead of approximating the measurements by line integrals[3]; (4) different grid sizes can be used in various parts of the plasma, in particular a large grid size in the bulk plasma, where the emission profile is relatively smooth, and a smaller grid size in the divertor, where small emitting structures may exist[4]; (5) the tomography method can give an estimate of the contribution of neutral particles to the divertor measurements if a sufficient number of measurements from outside the divertor is available [6,7]. The importance of these points, except for (5), is discussed below.

The performance of the tomography method and the effects of changing reconstruction parameters has been discussed in Ref. 10. Here, this is done for bolometry by means of phantom simulations. A phantom is a known emission profile, from which one can calculate what would be measured if the phantom were the actual emission profile (making use of the beam widths in this case). A realistic level of noise is added to these so-called pseudo-measurements (3% Gaussian noise relative to the measurement). The pseudo-measurements are then used as input in the tomographic reconstruction, the result of which is called tomogram. The tomogram can be compared directly with the phantom. The effect of varying reconstruction parameters can be studied objectively in this way, in contrast to actual measurement for which the actual emission profile is not known and one can only compare the backcalculated measurements ("pseudo-measurements" of the tomogram) with the actual measurement and use a subjective judgement

---

1 In fact, usually anisotropic "smoothness" is used as object function in the form of diffusion operators, see Refs. 10 and 11.

2 As will be demonstrated in the following discussion, a quadratic constraint in combination with limited coverage and very peaked divertor radiation leads to very negative artefacts in the tomographic reconstructions. Here, an efficient method to reduce or eliminate the negative values is employed [10,12]. Another way of finding a purely positive solution is, for example, with the entropy object function (the entropy of the reconstruction is maximized); this however is a computationally intensive highly non-linear technique.

3 In the line integral approximation the emission is assumed to be constant on planes perpendicular to the average line of sight within the beam width. The measured power is divided by the étendue of the detector and this value is assigned to the average line of sight (i.e. a point in projection space), see, for example, Ref. 8. Although this approximation is remarkably robust to violations of the basic assumption, taking into account the beam widths improves the reconstructions when the emission profile is very peaked, as will be demonstrated in the following.

4 Choosing the grid size equal in the entire plasma according to the requirements in the divertor is not necessarily problematic from the mathematical point of view, as the tomography method is properly regularized. However, one can argue that the grid size should be chosen according to the average distance between lines of sight in various parts of the plasma or according to the expected size of emitting structures to reduce the freedom of the tomography algorithm to create artefacts. This point is discussed in more detail later. At JET the main reason for implementing varying grid sizes was to reduce the required memory and computation time, which, for the current tomography method, scale with the second and third power, respectively, of the number of grid points.

on what one thinks the emission profile should look like. The phantoms used in this study are based on EDGE2D/NIMBUS predictions for a density-limit L-mode discharge in the MkIIA divertor, one in the attached and one in the detached phase. EDGE2D/NIMBUS only simulates the divertor, edge and scrape-of-layer. A realistic level of constant emissivity has been assumed in the bulk plasma. In the phantom simulations only lines of sight were used that are also available in reality and it was assumed that there is no contribution of neutrals particles to the signals.

3.2 Discussion of phantom simulations

The phantoms used in the phantom simulations are shown in Figs.4(a) and 5(a). Figure 4(b) shows the available lines of sights. Tomographic reconstructions with varying parameters for the detached phantom are shown in Figs.4(c–g,i) and the pseudomeasurements and backcalculated measurements from the best tomogram [Fig.4(c)] are given in Fig.6. The tomograms differ significantly when different reconstruction parameters are used, although the total radiated powers calculated from these tomograms do not vary much, as will be discussed in the next subsection.

For Fig.4(c) all beneficial features of the tomography code were exploited: beam widths were taken into account, anisotropic smoothness, non-negativity constraints and all available channels were used, and the reconstructions were carried out on a fine grid in the divertor. Obviously, much detail of the phantom has been lost due to a limited number of lines of sight, the beam widths, and smoothing in the tomographic reconstruction. The object function and constraint used to

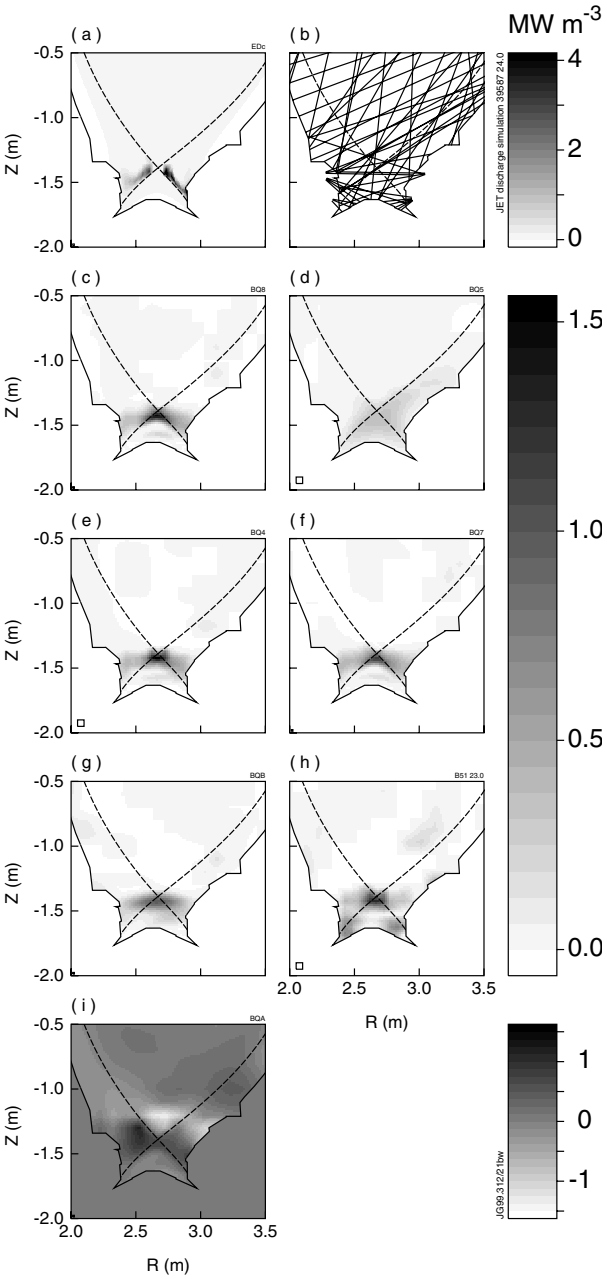

Fig.4: (a) Phantom of detached plasma (emission profile predicted by EDGE2D/NIMBUS code). (b) Lines of sight (in the divertor region) used in the reconstructions. (c–g,i) Tomographic reconstructions of pseudo-measurements with varying reconstruction parameters. (h) Tomographic reconstruction of actual measurements of the discharge simulated. The phantom simulations were done on a find grid in the divertor, with non-negativity constraint, with anisotropic smoothness, taking into account the beam widths and using all available channels, unless otherwise specified. (d) KB1 lines of sight only. (e) Coarse divertor grid. (f) Line integrals. (g) Isotropic smoothness. (i) No non-negativity constraints. The box in the lower-left corner indicates the grid size in the divertor, the green curve the separatrix of the plasma.

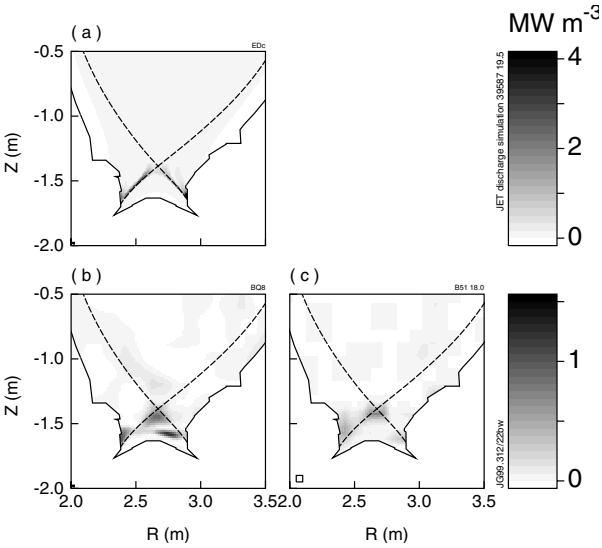

Fig.5: (a) Phantom of attached plasma. The peak values in the strike points are out of scale by about a factor of 2. (b) Tomographic reconstruction of pseudo-measurements (best result). (c) Tomographic reconstruction of actual measurements of the discharge simulated.

regularize the tomography problem lead to somewhat smoothed tomograms since the result of the reconstruction is the smoothest emission profiles that fits the measurements within the overall (i.e. not per channel) estimated errors, which leads to smoothing of peaks. This is a problem with virtually all tomography methods: the regularization requires the suppression noise, and this usually takes the form of suppression of high spatial frequency components as noise and genuine high-frequency components cannot be separated [13]. Although methods exist to enhance peaks in the tomogram [10], these only have a limited effect. The good fit of the backcalculated measurements to the pseudomeasurements in Fig.6 is no surprise as this is an input parameter of the reconstruction method (the discrepancy principle). In principle, the fit to the pseudomeasurements can be made as good as one wants (if there are enough grid points to allow this), but that is improper to require: noise in the measurements will cause unphysical artefacts in the tomogram[5]. Note that because the divertor emissivity is more than one order of magnitude higher than in the bulk plasma, small errors in the reconstruction lead to

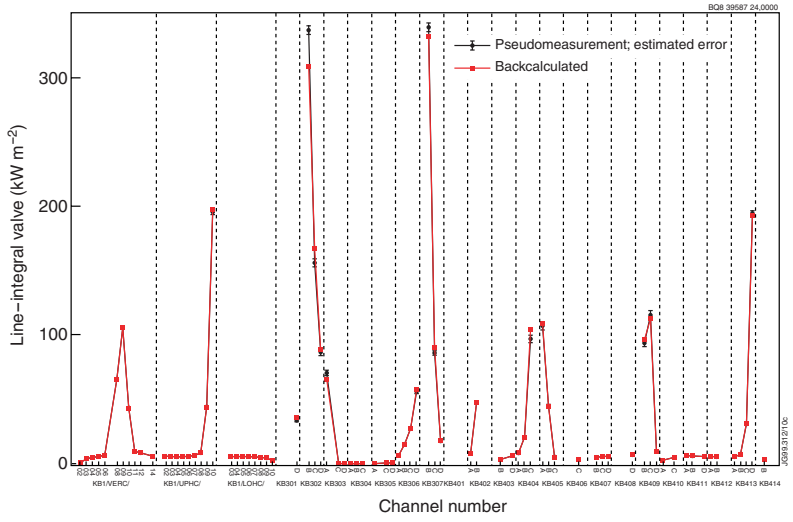

Fig.6: Pseudomeasurements and backcalculated measurements for the reconstruction of Fig.4(c) as a function of channel number (refer to Figs. 1–3 for the numbering).

5 This is related to the fact that the least-square solution of an ill-posed problem is not good in the presence of noise.

an unsmooth emissivity in the bulk plasma with very small values in places[6]. With the present lines of sight it is not possible to reconstruct accurately the emissivity in the bulk plasma from lines of sight that do not view the divertor without assumptions such as constant emissivity on flux surfaces, an assumption that usually is violated due to mainly an increase in radiation from the bulk plasma towards the divertor, and also due to in-out asymmetries.

If only the KB1 channels are taken into account [Fig.4(d)], the emitting peak in the divertor is smeared out even more due to the large beam widths and lacking spatial information in the divertor. A reconstruction with a grid with approximately a four times larger grid size in the divertor [Fig.4(e)] gives comparable results to those on the fine grid (although the convergence with non-negativity constraints is slower of even incomplete), indicating that for most purposes such a grid is adequate for this number of line of sight (tomographic reconstructions are significantly faster with fewer grid points). Neglecting the beam widths [Fig.4(f)], i.e. assuming that the measurements are along infinitely thin lines, leads to a significant underestimation of the peak values[7]. Taking pure isotropic smoothness as object function [Fig.4(g)] gives a smoother, less realistic result, indicating that anisotropic smoothness on flux surfaces is indeed a better object function. Finally, Fig.4(i) shows the dramatic effect of not using the non-negativity constraint, demonstrating that without non-negativity constraints the details of the emitting peaks are wrong and there are very large negative artefacts. Apparently these constraints are very important for a detection system with such irregular coverage, very localized peaks in the emissivity, and the other constraints in the tomography method being quadratic. This has been observed to be the case in many different types of JET plasmas and also in simulations for ITER [14]. Interestingly, application of the non-negativity constraint in tomographic reconstructions of ASDEX-Upgrade data has shown that for ASDEX-Upgrade data the constraint is much less important.

Figure 5(b) shows the best tomogram for the attached phantom. This reconstruction is worse than for the detached phantom (the convergence is also much slower). Apparently the coverage of the detection system is not sufficient to adequately characterize the attached emission profile, in particular the peaks at the strike points, whereas for the detached phantom the coverage is enough to yield a consistent reconstruction, albeit with much loss of detail.

Concluding, due to smoothing, the sparseness and the matching beam widths, much detail is lost in the reconstructions. The irregular coverage can also cause artefacts (as for the attached phantom) and a different resolution in various parts of the plasma. Even with much improved coverage it is very difficult to make very accurate reconstructions due to peakedness in divertor,

---

6 With a finite tolerance in the non-negativity constraint some values in the bulk plasma are somewhat negative, but in comparison with the positive values they are effectively zero.

7 Because the reconstruction with the full beam widths does not resemble the phantom in detail, one could argue that the difference between [Fig. 4(c)] and [Fig. 4(f)] is insignificant. However, for other, less structured phantoms it has been shown that taking into account beam widths in the bolometer reconstructions is indeed relevant [8].

as is exemplified in simulations done for the bolometer system proposed for ITER [14][8]. A successful way to derive improved detail is by sweeping the plasma in front of the detectors, thus creating many extra lines of sight from the time information of the sweep (provided only the position of the plasma and nothing else changes) [5,7,9].

3.3 Total radiated power calculation

The total radiated power can be calculated and compared for both the phantom and the tomograms of reconstructions with varying reconstruction parameters. Assuming toroidal symmetry, the total radiated power is the toroidal volume integral

$$P = 2\pi \iint g(R,Z)\, R\, \mathrm{d}R\, \mathrm{d}Z\,. \tag{2}$$

The main aim of this document is to compare the total radiated powers of tomograms obtained with different numbers of lines of sight and different reconstruction parameters and the total radiated powers obtained with techniques other than tomographic reconstructions (Sec. 4.2).

Table II Total radiated powers determined in different ways in phantom simulations. Unless otherwise specified, the fine divertor grid, the non-negativity constraint, anisotropic smoothness, and the beam widths were taken into account.

	Total radiated power (MW)	
Method	**Detached**	**Attached**
Phantom[a]	1.19	1.12
Tomography, KB1-only reconstruction	1.16	1.14
Tomography, all channels, coarse divertor grid	1.10	1.06
Tomography, all channels	1.09	1.03
Tomography, all channels, line integrals	1.16	1.19
Tomography, all channels, isotropic smoothness	1.13	1.11
Tomography, all channels, estimated noise 2×	1.08	1.07
Tomography, all channels, no non-negativity[b]	1.06 (4.9)	0.71 (6.1)
Tomography, all channels, inconsistent data	1.11	1.11
Weighted summation, unscaled p	0.94	0.88[c]
Weighted summation, scaled p	1.18	1.06[d]

[a] Depending on the grid on which the phantom is represented, a variation of up to 10% in total radiated power is found from the volume integral due to discretization errors.

[b] The values in brackets give the total radiation if negative values are neglected (set to zero).

[c] Corresponding to blue circles in Fig.8

[d] Corresponding to red squares in Fig.8

8 In these simulations it was found that even with significantly more lines of sight it is very difficult to reconstruct the emissivity in the bulk plasma reliable at the same time as one reconstructs the divertor radiation.

Table II gives the total radiated powers calculated with Eq. (2) for the various tomographic reconstructions given in Figs.4 and 5. Apparently, the total radiated power does not dependmuch (about 10%) on the number of lines of sight and modest variations in most reconstruction parameters. This robustness of the total power calculation has also been observed before in phantom simulations [14]. There are two exceptions to the robustness: (1) when no non-negativity constraints are used, and (2) from other cases than given in Table II (see the discussion of Fig. 10) inconsistent data can lead to artefacts that distort the total radiated power significantly. Usually, reconstructions without non-negativity constraints give reasonable total radiated power values if the negative emissivities are taken into account. If only the positive values are taken, hugely exaggerated total radiated powers are obtained[9] (in the given examples the negativity[10] was 0.4–0.6, whereas with the non-negativity constraint negativities smaller that 0.01 are obtained). Although the total radiated power obtained from reconstructions without the non-negativity constraint usually is reasonable, it cannot be relied upon as the attached case in Table II illustrates.

4. WEIGHTED SUMMATION

4.1 Background

The area integral

$$\tilde{P} = \iint g(R,Z)\,\mathrm{d}R\,\mathrm{d}Z = \int f(p,\xi)\,\mathrm{d}p \tag{3}$$

is true independent of angle ξ: all vertical integrals of the sinogram are equal[11]. Relating Eq. (3) to the toroidal volume integral of Eq. (2), one can write

$$P = 2\partial \int f(R,\xi=\pi/2)\,R\,\mathrm{d}R \approx 2\pi R_0 \tilde{P}, \tag{4}$$

where R has been identified with p for $\xi=\pi/2$. For a machine with the aspect ratio of JET, the approximation with the constant R_0 is not bad: it only deviates some per cent from the proper integral over R. The consequence of Eqs. (3) and (4) is that if measurements exist on or can be mapped to any $\xi = \text{const}$ line, a reasonable approximation of the total radiated power can be obtained from the integral along this line. This procedure is highly preferable to calculating the total radiated power from a tomographic reconstruction as it is a robust integral method, whereas the tomographic reconstruction is a noise-sensitive differential operation (ill-posed problem)[12].

---

9 Taking only positive values is inappropriate because the backcalculated values from the positive values of the tomogram are much higher than the measurements, i.e. the positive tomogram is inconsistent with the measurements.

10 The negativity is defined as the square root of the summed square of negative values over the summed square of all values.

11 Equation 3 can be considered as a zeroth moment (p^0); similar ξ -independent properties of the sinogram can be derived for higher moments of p [13]; these are sometimes referred to consistency conditions for the sinogram.

12 If the tomographic reconstructions has artefacts, the location of the artefacts may give rise to incorrect total radiated power values calculated from the reconstruction.

Discretization of Eq. (4) gives

$$P \approx 2\pi R_0 \sum_i f(p_i, \xi = \text{const})\,\Delta p_i\,. \tag{5}$$

Equation (5) will be referred to as the weighed-summation method to determine the total radiated power, the weights being given by Δp_i between the discrete measurements. If measurements existed along a line $\xi = \text{const}$ (i.e. parallel lines of sight covering the entire cross-section), only discretization errors and an error due to constant R_0 would be made with this method. In reality, however, no such measurements exist on JET and many other tokamaks [Fig.7(a)]. The set of measurements closest to $\xi = \text{const}$ is the vertical camera of KB1 (KB1V). Because the channels of KB1V share a common aperture with coordinates $(R_{\text{ap}}, Z_{\text{ap}})$, the projection-space points corresponding to the average lines of sight $(\overline{p}_i, \overline{\xi}_i)$ lie on the "aperture curve" [Fig.7(b)]

$$p_{\text{ap}}(\xi) = -(R_{\text{ap}} - R_0)\sin\xi + (Z_{\text{ap}} - Z_0)\cos\xi\,. \tag{6}$$

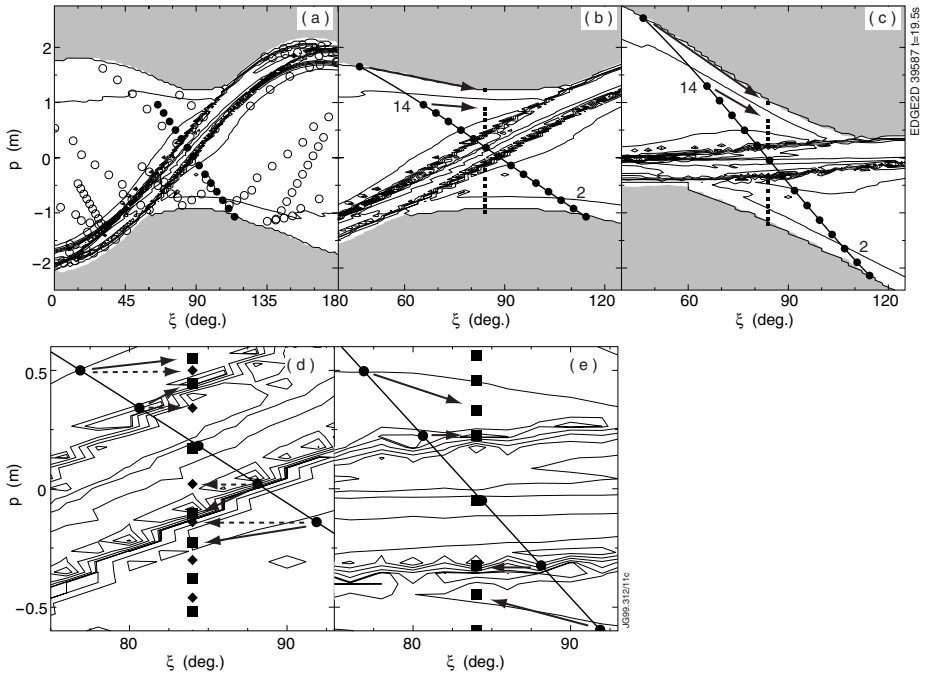

Fig.7: Contour plots of the sinogram for the phantom with attached plasma [Fig.5(a)]. The grey area is the area of projection space where lines of sight do not pass inside the JET vessel. (a,b,d) Origin of projection space on nominal magnetic axis. (c,e) Origin of projection space in X point. (a) Solid circles: average lines of sight of the KB1 vertical camera; open circles: average lines of sight of the other KB1, KB3 and KB4 channels. (b,c) Blow up of (a); curve: aperture curve of the KB1 vertical camera; solid circles: channels of KB1 vertical camera plus a virtual (zero) channel just outside the boundary; solid squares: lines of sight projected onto the line $\xi = 84°$ *with scaled* p. *(d,e) Blow up of (b,c); solid diamonds: lines of sight projected onto the line* $\xi = 84°$ *with* un*scaled* p. *The solid arrows in (b,c,d,e) show the projection process onto* $\xi = 84°$ *with scaled* p *for some lines of sight. The dashed arrows in (d) show the projection process onto* $\xi = 84°$ *with* un*scaled* p. *The of the contour plots are not equidistant to enhance lower values (of the bulk plasma). The ragged shape of the contours is due to the coarseness of the* (p, ξ) *grid used.*

The main problem in applying the weighted summation method to JET data (and data from other tokamaks) is that an accurate mapping from the aperture curve to a $\xi = \text{const}$ line has to be found. Two ways of doing this are indicated in Fig.7(b–e) and will be discussed next. Two approaches to finding appropriate weights for the weighted summation are discussed: (1) determination from sinograms (Subsection 4.2) and (2) a statistical approach (Subsection 4.4).

4.2 Weights determined from the sinogram

The $\xi = \text{const}$ line chosen in the following is $\xi = 84°$, which is centred on the KB1V line of sight viewing the centre of divertor. This seems slightly more appropriate than $\xi = 90°$, but one loses the benefit of the more exact calculation of the first equality in Eq. (4). The simplest method to map the aperture curve to a $\xi = \text{const}$ line is to keep the p constant (unscaled p), and just change the ξ to $\xi = \text{const}$. Figure 8 shows the cross-section of the sinogram of Fig.7 at $\xi = 84°$ (solid black curve) and the projection of the sinogram values along the aperture curve to $\xi = 84°$ with unscaled p (dotted green curve). For p<–0.5m and p>1.0m it is clear that due to the elongated shape of the plasma the sinogram is "squeezed" around $\xi = 90°$, and therefore it is appropriate to apply this squeezing in the mapping [arrows in Fig.7(b)], which results in a scaled p. Close to the X-point the scaling in this way is very slight [diamonds and dashed arrows in Fig.7(d)]. This mapping is satisfactory for the bulk plasma, for example in the limiter phase of a discharge. However, from Fig.7(d) and the dotted green curve in Fig.8 it is evident that this mapping is unsatisfactory at the X point: the extent of the X-point radiation is underestimated, which would lead to too low a total radiation. An improved mapping is indicated by the solid arrows in Fig.7(d). A convenient way to formulate this mapping is in projection space of which the origin lies in the divertor or X point [Figs.7(c,e)]: in these coordinates (p', ξ') the three central channels are

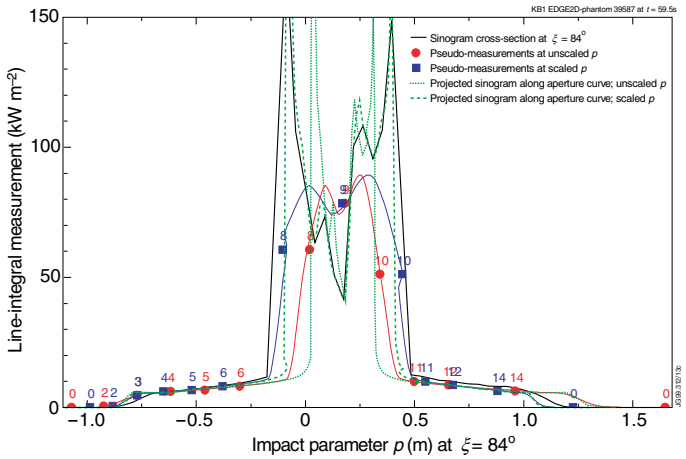

Fig.8: Cross-section of the sinogram (solid black curve), projected sinogram curves (green) and projected pseudo-measurements (red and blue points), all at $\xi = 84°$. The red circles and the dotted green curve are projected with unscaled p*, whereas the blue squares and the dashed green curve are projected with scaled* p*. The red and blue curve through the points is the convolution of the dotted green or dashed green curve, respectively, with the normalized nominal angular étendue of the system (instrument function, see Sec. 5).*

mapped with unscaled p', whereas the other channels are squeezed proportionally to their distance from $\xi = 84°$. This leads to the improved mapping of the dashed green curve in Fig.8. The effect on the pseudomeasurements (including the beam widths) is given by the red squares with respect to the blue circles. The total radiated power values obtained with weighted summation with unscaled and scaled p are given in Table II. As expected, the values obtained with unscaled p are far too low, while the values obtained with scaled p are very reasonable.

The dashed green curve in Fig.8 could still be broadened further to be closer to the actual values (black curve). However, although the scaling is *ad hoc*, there is a clear justification for it from the sinograms, whereas there is no real justification for further broadening. Furthermore, for other phantoms, for example the detached phantom, in which case there is much radiation from around the X point, the width of the dashed green curve coincides better with the black curve. It seems therefore, that more accurate mappings cannot be independent of the radiation profile.

It is remarkable that although the three central lines of sight of KB1V seem virtually parallel in the divertor, the fan-shape distribution has a major impact on the scaling of p that has to be applied in the mapping from the aperture curve to $\xi = \text{const}$. Not the peakedness of the divertor radiation is the problem, but the divergence of the lines of sight! Therefore, it can be concluded that the calculated total radiated power will not depend strongly on the peakedness of the divertor radiation, but rather on the broadness and on the ratio of divertor to bulk radiation. Because the sinogram is given by the line integrals, it mixes bulk radiation (which requires a squeezed mapping of p) with divertor radiation (which requires an expanded mapping of p close to the X point). It is clear that it may be difficult to find a single set of weights Δp_i in Eq. (5) that gives satisfactory results for widely different plasmas, as will become clear from the following.

4.3 Comparison with BOLO/TOPO

The current quick total radiated power calculation used at JET, called BOLO/TOPO, has been applied for a long time, and its results have been found to be satisfactory. However, its values in the divertor phase of discharges have been found to be consistently lower than those found by tomography by up to 10% (consistent with the errors found in Sec. 3), which has been assumed to indicate what the error bars of this simple calculation method are. The methods with unscaled p and scaled p have been compared with BOLO/TOPO for range of plasmas in the JET MkI, MkIIA and MkIIGB divertors, and it has been found that the in most cases BOLO/TOPO is close to the method with unscaled p, and that the method with scaled p gives higher values. In the limiter phase unscaled p gives higher values than BOLO/TOPO because the elongation is not taken into account in the former method, but it is in the latter; whereas the effects of the elongation of the bulk plasma becomes negligible in the divertor phase as the emission in the divertor dominates. Therefore, it can be concluded that the algorithm of BOLO/TOPO gives similar results as a weighted summation method with squeezed p, but no expansion at the X point. To assess which simple method gives the most reliable results, the methods mentioned

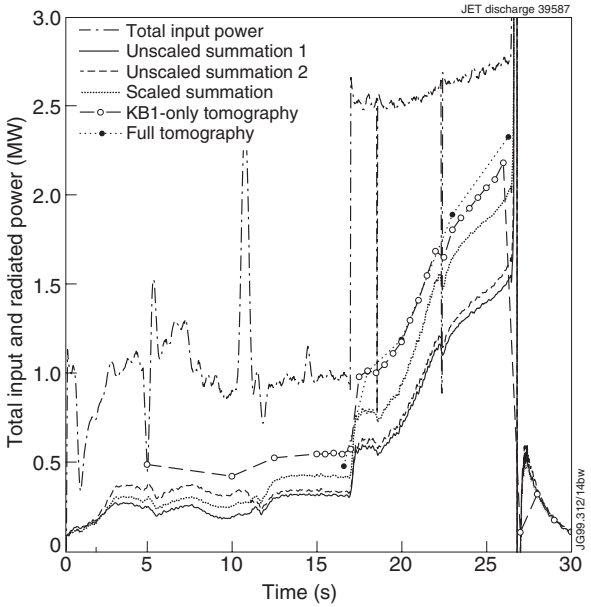

Fig.9: Total radiated power calculated by the various methods for an L-mode density-limit discharge in the MkIIA divertor (incidentally, the same discharge that was simulated by EDGE2D, which emission profiles were used as phantoms in this study).

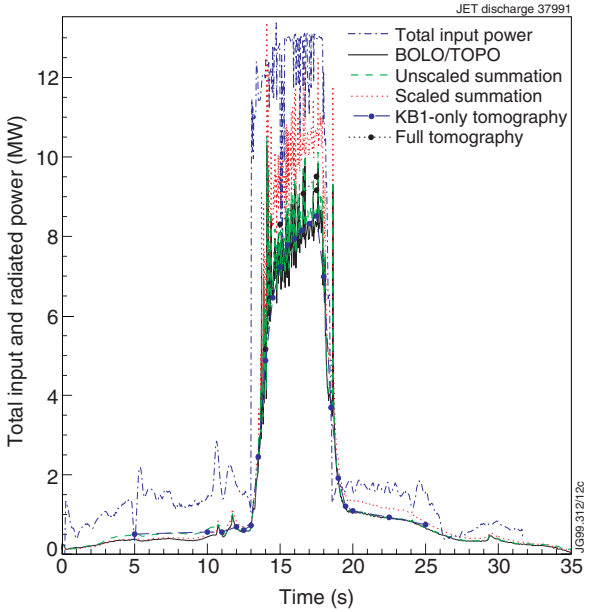

Fig.10: Total radiated power calculated by the various methods for an H-mode impurity-seeded density-limit discharge in the MkIIA divertor.

above have been compared for a small number of discharges with tomographic reconstructions using (1) KB1 channels only, and (2) all available bolometers. Figures 9 and 10 show two examples. In Fig.9 (an L-mode density-limit discharge) it is found that, as in most other cases studied, BOLO/TOPO and the method with unscaled p are lower than the more reliable values form the tomographic reconstructions and the method with scaled p, while the tomographic reconstructions and the method with scaled p agree fairly well (the spread is an indication of the error bars that have to be assumed). Figure 9 is an extreme example in which BOLO/TOPO and the method with unscaled p are much lower (almost 30%) than the more reliable values. However, the method with scaled p is not always a better estimate than with unscaled p: Fig.10 (an impurity-seeded H-mode density-limit discharge; data averaged over ELMs) shows that in some cases BOLO/TOPO agrees much better with the tomographic reconstructions than the method with scaled p. The reason for such different behaviour is not entirely clear. Figure 11 shows that, if the signals are normalized to the central channel of the vertical camera, the radiation in the divertor in the case of Fig.9 is somewhat broader than the case of Fig.10, that the bulk radiation in the latter is significantly higher and that the X-point radiation in the former is much higher (clear from the UPHC camera) and extends further in (Fig.9 is for a plasma with vertical targets, whereas Fig.10 is with horizontal targets; the X point in the former is therefore higher up). Hence, it is possible that the scaling of p found for the case of Fig.9 with the higher X point overestimates the total radiated power in the case of Fig.10. These results indicate that it seems impossible to find one set of weights Δp_i in Eq. (5) that gives satisfactory results for widely different plasmas. The cause for the significant difference in Fig.10 between KB1-only

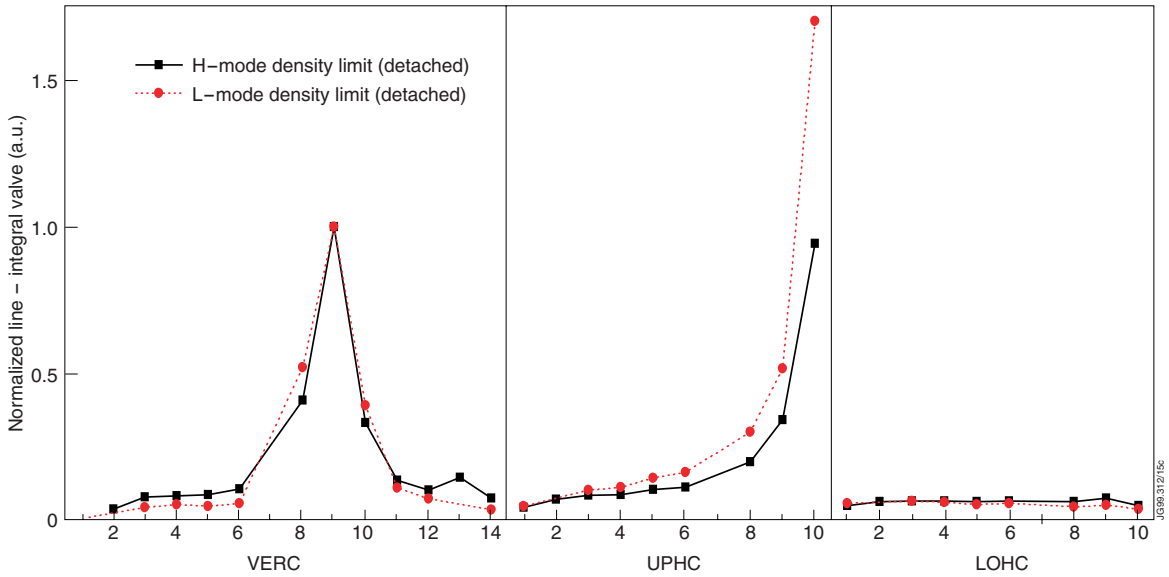

Fig.11: KB1 measurements as a function of channel number for one timeslice in two discharges (the red circles correspond to t=24.0s in Fig 9; the black squares to t=16.6s in Fig.10). The line-integral values have been normalized to channel KB1V9 to make a relative comparison possible. The channel numbering is according to Fig.1.

reconstructions and reconstructions with all channels is thought to be an artefact in the bulk plasma in the latter reconstructions that is caused by inconsistencies in data (measured values or uncertainties in the alignment of lines of sight). An important inconsistency in the data is due to the KB1 cameras being in different octants: one horizontal camera often observes a significant increase in radiation in the upper-inner corner as a result of plasma-wall interaction.

4.4 Statistical approach to finding weights

Given the finding that the tomographic reconstructions give reliable values for the total radiated power (Sec. 3), it is possible to find weights of the summation by fitting the weights so that the summation gives the total radiation known from tomography. Statistical methods can be used to find appropriate weights for a wide range of discharges. Such a method has been applied at ASDEX-U [15]. Also, a neural network could be trained for this purpose. To successfully apply such statistical methods, a large database with reliable results for widely varying plasma parameters is required to find appropriate weights or to train the neural network. Unfortunately, as at JET the only reliable way to obtain the total radiated power is by tomographic reconstructions of carefully verified bolometer measurements, the database currently available is too small. A major effort would be required to build such a database and to derive the optimum weights by a statistical method. In view of Fig.11, improved results may be obtained in the statistical approach if not only KB1V channels are used in the weighted summation, but also other KB1 channels are taken into account.

5. EFFECTS OF BLURRING

In Fig.8 the blurring, or smoothing, effect of the instrument function is evident. It is worthwhile to investigate the information loss due to the blurring and whether this can affect the total radiated

power that is determined. It is convenient to do this investigation along the aperture curve, i.e. the curve of which the points correspond to lines that go through the centre of the common aperture of the detectors [see Fig.7(b)]. The instrument function can be approximated along this curve by the angular étendue [8], which is defined as

$$e_i(\xi) = \int k_i(p,\xi)\,\mathrm{d}p, \tag{7}$$

where i numbers the detector and $k_i(p,\xi)$ is the geometric function in projection space [8]. The étendue for the average angle $\bar{\xi}_i$ is given by [8]

$$E_i(\bar{\xi}) = \int_0^{\pi} \frac{e_i(\xi)}{\cos(\xi - \bar{\xi}_i)}\,\mathrm{d}\xi. \tag{8}$$

In the following, normalized angular étendues $\bar{e}_i(\xi) = e_i(\xi)/E_i(\bar{\xi}_i)$ have been used, so that the dimensions of both unblurred and blurred line integrals are the same. Because the angles for which $e_i(\xi)$ is nonzero are very close to $\bar{\xi}_i$, the cosine in the denominator of the integrand in Eq. (8) is close to one and the integral $\int \bar{e}_i(\xi)\,\mathrm{d}\xi \approx 1$. The normalized angular étendues of the KB1V channels are shown in Fig.12(b). These angular étendues of all channels are virtually identical; the reason for the variation in width and height is a cosine-effect due to the angle at which the various detectors view through the aperture. Because the instrument function of all channels can be assumed to be represented by the one of one particular channel, $\bar{e}(\xi)$, one can write the blurring as the convolution

$$\hat{f}(p_{ap}(\xi),\xi) = \int f(p_{\mathrm{ap}}(\xi'),\xi')\,\bar{e}(p_{\mathrm{ap}}(\xi-\xi'),\xi-\xi')\,\mathrm{d}\xi', \tag{9}$$

and pseudomeasurements are given by $\hat{f}_i = \hat{f}(p_{\mathrm{ap}}(\bar{\xi}_i),\bar{\xi}_i)$. Because $\int \bar{e}(\xi)\,\mathrm{d}\xi \approx 1$, it follows that

$$\int \hat{f}(p_{\mathrm{ap}}(\xi),\xi)\,\mathrm{d}\xi \approx \int f(p_{\mathrm{ap}}(\xi),\xi)\,\mathrm{d}\xi, \tag{10}$$

which means that no "power" is lost due to the blurring in a "total" power[13] calculation along aperture curve. Note, however, that an uncertainty in the total power is introduced by the coarseness of the sampling and by the nonlinear scaling and mapping of Sec. 4.2.

Figure 12 shows the effect of blurring by the instrument function (angular étendue) for the sinogram values along the aperture curve. In Fourier space (for the coordinate along the aperture curve) the effect of the blurring and of the limited sampling by the detectors is very clear. The values for $\Xi < 0.1\ \mathrm{deg}^{-1}$ correspond to the peak of radiation in the divertor, whereas peaks for $\Xi > 0.15\ \mathrm{deg}^{-1}$ correspond to the fine structure. In this example (the attached EDGE2D phantom)

13 The integral along the aperture has no direct physical meaning, but the fact that it is not strongly affected by the instrument functions indicates that the same should be true for the projection to constant ξ, and it is therefore related to the total radiated power.

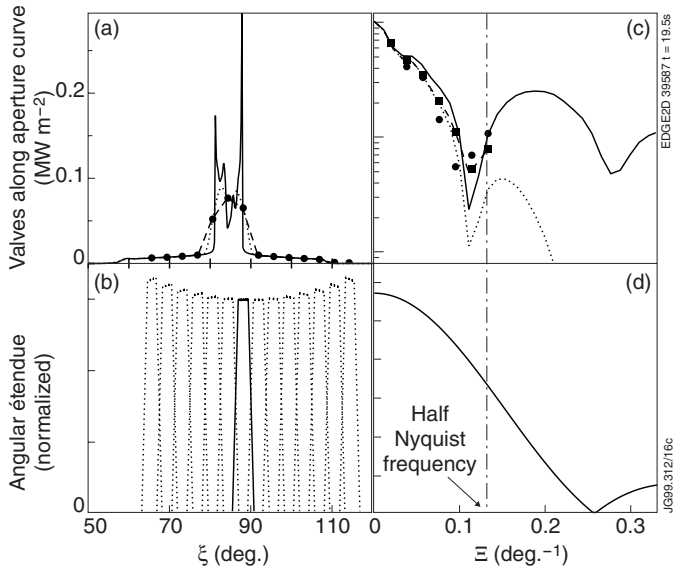

Fig.12: Quantities along aperture curve for the attached phantom as a function of the angle ξ (a,b) and its Fourier counterpart Ξ (c,d). (a) Sinogram values: solid line: line-integral values; dotted line: values blurred by instrument function; filled circles: points where the blurred values are sampled (pseudomeasurements corresponding to the detectors); dashed curve: piecewise-linear fit to sampled points. (b) Angular étendue (instrument function along aperture curve) normalized to the étendue for the KB1V detectors; the one used in the investigation is given by the solid line. (c,d) Fourier transforms of (a) and (b), respectively, with equivalent linetypes and symbols. Note that (c) is on a logarithmic scale and (d) on a linear scale. Although the Fourier transforms were carried out with the discrete Fourier transform (DFT), the number of samples was chosen such that the figures are a good representation of the analytical Fourier transform, with the exception of the DFT of the pseudomeasurements (filled circles). The DFT of the pseudomeasurements is numerically inaccurate due to the small number of samples and the fact that the samples do not extend over the entire range of the plasma. The dashed curve in (c) indicates the blurred function aliased with values higher than half the Nyquist frequency (vertical dot-dashed line at $\Xi = 0.13\ \mathrm{deg}^{-1}$); the filled squares on this curve indicate the theoretical samples one would expect to find instead of the inaccurate filled circles.

the peak at $\Xi \approx 0.2\ \mathrm{deg}^{-1}$ is not sufficiently damped by the instrument function which leads to considerable aliasing. However, the amplitudes that are affected by the aliasing are relatively small, about a factor of 5 below the zero frequency component.

The Fourier transform of $\hat{f}$ along the aperture curve is given by[14]

$$\hat{F}(\Xi) = \int \hat{f}(p_{\mathrm{ap}}(\xi), \xi) \exp(-2\pi i \xi \Xi)\, d\xi .$$

Noting that $\hat{F}(0)$ is equal to the "total" power along the aperture curve [Eq. (10)], it is clear that the zero frequency component carries the total power and that also in the Fourier domain the blurring (filtering at higher frequencies) has no effect on the total power if the signal is continuous. However, sparse sampling complicates the interpretation of $\hat{F}(0)$: due to aliasing $\hat{F}(0)$ may be incorrect. This is related to the observation in that integration over a piecewise

14 Note that although the variable ξ is periodic, and hence the corresponding frequency variable would be *discrete*, here the periodicity of ξ is irrelevant because the function that is Fourier transform goes to zero at both low and high ξ. Therefore, the frequency variable Ξ considered here is continuous.

linear fit to the measuring points of Fig.12(a), i.e. a trapezoidal rule, may overestimate or underestimate the proper integral over the blurred curve. Because the regions where the piecewise linear fit is higher or lower than the blurred curve will largely cancel unless the sampling is extremely sparse with respect to the beam widths, the effect on $\hat{F}(0)$ will be small [as is also clear from the minimal aliasing at $\Xi = 0\,\mathrm{deg.}^{-1}$ in Fig.12(c)].

The instrument functions of neighbouring channels overlap close to their half-maximum values [Fig.12(b)]. This seems optimal as no emitting peaks between channels can be missed. However, the Fourier transform of the angular étendue has its first zero only at the Nyquist frequency $1/\Delta\xi$, where $\Delta\xi$ is the spatial sampling rate [see Fig.12(d)]. Therefore, with this kind of limited overlap between instrument functions, significant aliasing can occur [16,17,18], see Fig.12(c). The lobes of the Fourier transform of the angular étendue are so small, that hardly any aliasing would occur if the overlap of the instrument functions were twice the current (i.e. the first zero of the Fourier transform of the angular étendue would coincide with half the Nyquist frequency). However, this would lead to a significantly reduced spatial resolution. Furthermore, Fig.12(c) is an extreme case as in other cases, such as the detached EDGE2D phantom, the aliasing effect is much smaller. Therefore, the current overlap between the instrument functions appears to be a reasonable compromise between maximizing resolution and minimizing aliasing. However, one should always remember that aliasing can occur.

As has been indicated, it is possible to obtain improved resolution by sweeping the plasma [5,7,9]. The emission profile not blurred by beam-width effects can then be restored to a certain extent by deconvolution [18].

6. CONCLUSIONS

Calculating the total radiated power from properly regularized tomographic reconstructions is fairly reliable and is quite insensitive to most reconstruction parameters and the number of lines of sight used for the reconstructions (as long as the lines of sight used are consistent and contain a sufficient amount of information about the entire plasma cross-section). Inconsistencies in the data and not using a non-negativity constraint in the reconstructions, however, can severely affect the result. Unfortunately, tomographic reconstructions are too time-consuming to be carried out for several time slices of each discharge, and should also be checked by hand.

A simpler and far more efficient calculation is possible by a weighted summation. The properties of such a weighted summation were studied in a fundamental way in projection space. The results for the JET bolometer system are thought to be valid for similar weights determined in other ways, for example by statistical methods, as well. It was found that the weights of the weighted summation depend on the profile shape of the emissivity, in particular the divertor radiation, and it does not seem to be possible to obtain a robust set of weights that gives accurate total radiated powers for widely different plasmas. The limitations to the method seem to stem from the combination of a local peak of radiation in the divertor and the fan-distribution of the

lines of sight (the total radiated power determined from truly parallel lines of sight should not suffer from these problems). Finding weights for separate classes of plasmas, for example with statistical methods, would be a lot of work and not necessarily be more reliable that the present calculation. The standard weighted summation calculation at JET (BOLO/TOPO) was determined to be accurate within 10% for most plasmas (usually BOLO/TOPO underestimates the total radiated power), but for some plasmas the total radiated power may be underestimated by as much as 30%. Beam widths of the measuring system (the instrument function) do not significantly affect the total radiated power determined by a weighted summation.

ACKNOWLEDGEMENTS

The author is grateful to Dr. C.F. Maggi for the EDGE2D/NIMBUS simulations that gave the emission profiles that were used as phantoms, and to Dr. J.C. Fuchs for discussions on methods to determine the total radiated power and for a collaboration on the determination of the relevance of the non-negativity constraint. The algorithm for the BOLO/TOPO calculation has been programmed, modified and tested by Drs. K.F. Mast, N.A.C. Gottardi, H.J. Jäckel and R. Reichle.

REFERENCES

[1] J.C. Fuchs, Max-Planck-Institut für Plasmaphysik, Garching, Germany; private communication

[2] E.R. Müller and F. Mast, "A new metal resistor bolometer for measuring vacuum ultraviolet and soft x radiation," J. Appl. Phys. **55**, 2635–2641 (1984)

[3] K.F. Mast and H. Krause, "Bolometric diagnostics in JET," Rev. Sci. Instrum. **56**, 969–971 (1985)

[4] K.F. Mast *et al.*, "A low noise highly integrated bolometer array for absolute measurement of VUV and soft x radiation," Rev. Sci. Instrum. **62**, 744–750 (1991)

[5] Reichle *et al.*, "Low energy neutral particle fluxes in the JET divertor," J. Nucl. Mat. **241–243**, 456–461 (1997)

[6] L.C. Ingesson *et al.*, "Radiation distribution and neutral-particle loss in the JET MkI and MkIIA divertors," in *Proceedings of the 24th EPS Conference on Controlled Fusion and Plasma Physics (Berchtesgaden)*, Ed. M. Schittenhelm *et al.*, Europhysics Conference Abstracts Vol. 21A (EPS, 1997), Part I, pp. 113–116

[7] L.C. Ingesson *et al.*, "Radiation distribution and neutral-particle loss during detachment in JET," in *Proceedings of the 26th EPS Conference on Controlled Fusion and Plasma Physics (Maastricht)*, Europhysics Conference Abstracts Vol. 23J (EPS, 1999), pp. 257–260

[8] L.C. Ingesson *et al.*, "Projection-space methods to take into account finite beam-width effects in two-dimensional tomography algorithms," J. Opt. Soc. Am. A **16**, 17–27 (1999); see also JET Report JET-R(98)02

[9] J.C. Fuchs *et al.*, "Radiation distribution and power balance in the ASDEX Upgrade Lyra divertor," in *Proceedings of the 1998 International Conference on Plasma Physics and the 25th EPS Conference on Controlled Fusion and Plasma Physics (Prague)*, Ed. P. Pavlo, Europhysics Conference Abstracts Vol. 22C (EPS, 1998), pp. 1510–1513

[10] L.C. Ingesson *et al.*, "Soft x ray tomography during ELMs and impurity injection in JET," Nucl. Fusion **38**, 1675–1694 (1998)

[11] J.C. Fuchs *et al.*, "Twodimensional reconstruction of the radiation power density in ASDEX Upgrade," in *Proceedings of the 21st EPS Conference on Controlled Fusion and Plasma Physics (Montpellier)*, Ed. E. Joffrin et al., Europhysics Conference Abstracts Vol 18B (EPS, 1994), Part III, pp. 1308–1311

[12] G.C. Fehmers, L.P.J. Kamp and F.W. Sluijter, "An algorithm for quadratic optimization with one quadratic constraint and bounds on the variables," Inv. Problems **14**, 893–901 (1998)

[13] R.M. Lewitt, "Reconstruction methods: transform methods," Proc. IEEE **71**, 390–408 (1983)

[14] L.C. Ingesson and R. Reichle, *Lines of sight for ITER bolometers*, JET Report JET-R(98)03

[15] M. Maraschek *et al.*, "Real-time determination of total radiated power by bolometric cameras with statistical methods," Rev. Sci. Instrum. **69**, 109–115 (1998)

[16] A. Macovski, "Physical problems of computerized tomography," Proc. IEEE 71, 373–378 (1983)

[17] A.G. Lindgren and P.A. Rattey, "The inverse discrete Radon transform with applications to tomographic imaging using projection data," Advances in Electronics and Electron Physics **56**, 359–410 (1981)

[18] R.N. Bracewell, "Correction for collimator width (restoration) in reconstructive x-ray tomography," J. Comput. Assisted Tomogr. **1**, 6–15 (1977)